

Structural Insights into the Function of the Nicotinate Mononucleotide:phenol/*p*-cresol Phosphoribosyltransferase (ArsAB) Enzyme from *Sporomusa ovata*

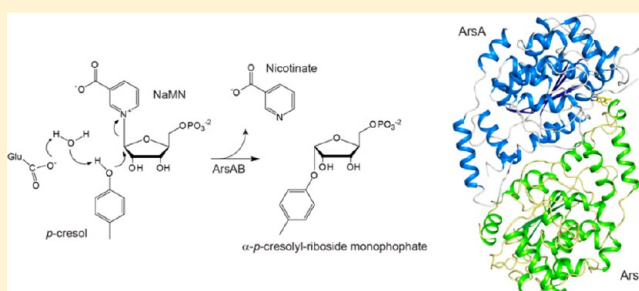
Sean A. Newmister,^{†,§} Chi Ho Chan,^{‡,§} Jorge C. Escalante-Semerena,^{*,‡,#} and Ivan Rayment^{*,†}

[†]Departments of Biochemistry and [‡]Bacteriology, University of Wisconsin, Madison, Wisconsin 53706, United States

[#]Department of Microbiology, University of Georgia, Athens, Georgia 30602, United States

Supporting Information

ABSTRACT: Cobamides (Cbas) are cobalt (Co) containing tetrapyrrole-derivatives involved in enzyme-catalyzed carbon skeleton rearrangements, methyl-group transfers, and reductive dehalogenation. The biosynthesis of cobamides is complex and is only performed by some bacteria and archaea. Cobamides have an upper (*Coβ*) ligand (5'-deoxyadenosyl or methyl) and a lower (*Coα*) ligand base that contribute to the axial Co coordinations. The identity of the lower *Coα* ligand varies depending on the organism synthesizing the Cbas. The homoacetogenic bacterium *Sporomusa ovata* synthesizes two unique phenolic cobamides (i.e., *Coα*-(phenolyl/*p*-cresolyl)-cobamide), which are used in the catabolism of methanol and 3,4-dimethoxybenzoate by this bacterium. The *S. ovata* ArsAB enzyme activates a phenolic lower ligand prior to its incorporation into the cobamide. ArsAB consists of two subunits, both of which are homologous (~35% identity) to the well-characterized *Salmonella enterica* CobT enzyme, which transfers nitrogenous bases such as 5,6-dimethylbenzimidazole (DMB) and adenine, but cannot utilize phenolics. Here we report the three-dimensional structure of ArsAB, which shows that the enzyme forms a pseudosymmetric heterodimer, provide evidence that only the ArsA subunit has base:phosphoribosyl-transferase activity, and propose a mechanism by which phenolic transfer is facilitated by an activated water molecule.



Cobamides are cobalt-containing modified cyclic tetrapyrrole-derivatives, which are members of a broad family that include all forms of heme (iron), chlorophylls (magnesium), and coenzyme F₄₃₀ (nickel).¹ Several features distinguish cobamides from other members of this family of molecules. As depicted in Figure 1, a cobamide has an upper (*Coβ*) ligand covalently bound to the cobalt ion of the ring, and a lower (*Coα*) ligand interacting with the Co ion via a coordination bond.

Vitamin B₁₂ is a cobamide (Cba) that contains a cyano (CN) group as the *Coβ* ligand (Figure 1). When DMB is the *Coα* ligand, it is known as cyanocobalamin. Cobamides are in their coenzymic form when the *Coβ* ligand is 5'-deoxyadenosine (AdoCba). AdoCba participates in radical mediated molecular rearrangement such as in diol dehydratase and methylmalonyl-CoA mutase.^{2,3} Cobamides also serve as transient methyl-group carriers in Co(I)Cba-dependent methyltransferases.⁴ In nature, the nucleoside base of cobamides varies, depending on the microorganism synthesizing it.^{5,6} Purines and purine analogues linked to the ribosyl group via an *N*-glycosidic bond can form coordination bonds with the cobalt ion, while bases linked to the ribosyl group via an *O*-glycosidic bond cannot (Figure 1B,C).

Only some bacteria and archaea synthesize cobamides,⁷ and unique among cobamides are those with phenol or *p*-cresol as

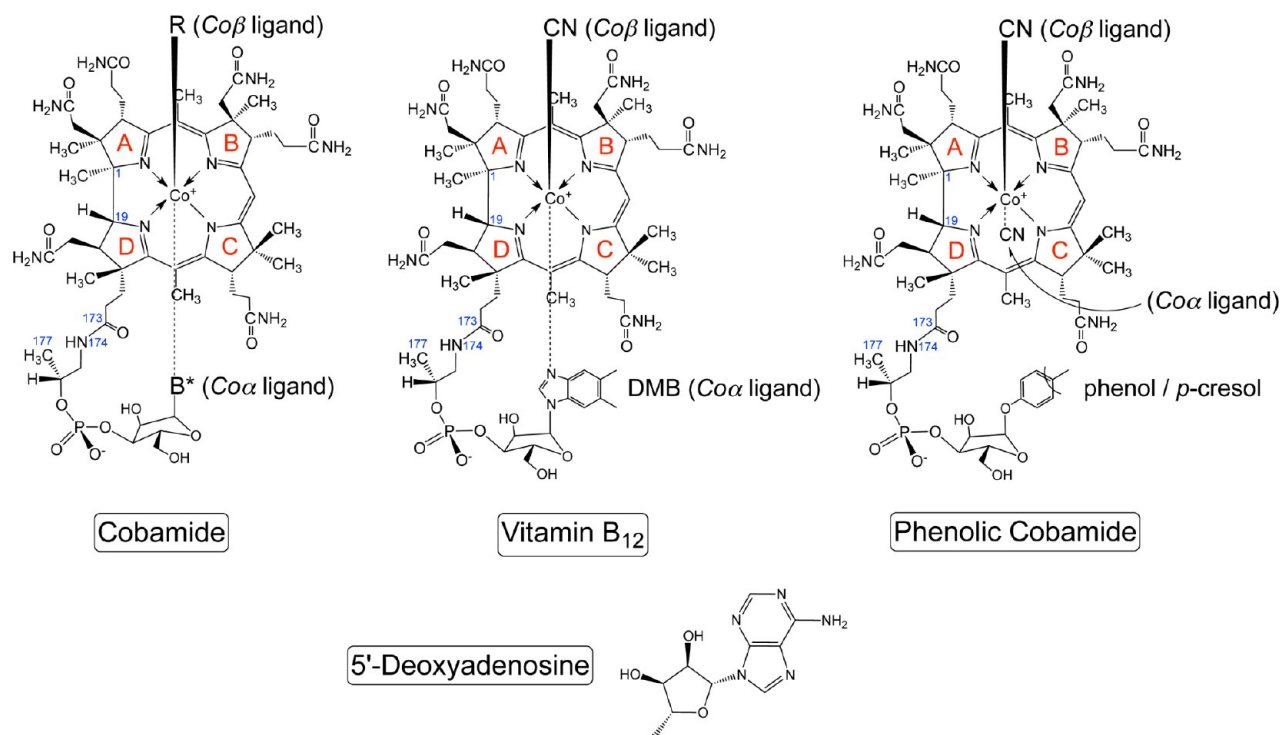
the lower ligand (Figure 1C). Phenolic cobamides were first described in the homoacetogenic bacterium *Sporomusa ovata*.^{8,9} Two features of the *S. ovata* cobamides are of note. First, the phenolic compound is covalently attached to the ribosyl group via an *O*-glycosidic bond, rather than the *N*-glycosidic bond found in all other known cobamides; second, unlike any other cobamides, phenolic cobamides cannot exist in the 'base-on' conformation because neither phenol nor *p*-cresol contains an atom that can establish a coordination bond with the Co ion of the corrin ring. Enzymes that require cobamides in the base-on conformation for catalysis (e.g., glycerol dehydratase, diol dehydratase, ethanolamine ammonia-lyase) cannot use or are inhibited by phenolic cobamides.^{10,11}

Recently, the *S. ovata* *arsAB* genes encoding the two subunits of the enzyme responsible for the conversion of phenol/*p*-cresol to the corresponding α -*O*-glycosidic riboside monophosphate were identified. The *arsAB*-encoded enzyme was isolated to homogeneity, and initial analyses of its activity were performed *in vivo* and *in vitro*.¹² The enzyme functions as a heterodimer; i.e., neither subunit is active by itself. The two

Received: August 23, 2012

Revised: October 5, 2012

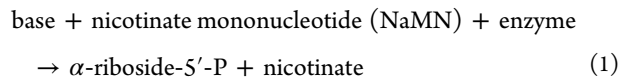
Published: October 5, 2012



When 5'-deoxyadenosine is the upper ligand, the cobamide is in its coenzymic form

Figure 1. Chemical structures of cobamides, vitamin B₁₂, and phenolic cobamides. The upper Co β ligand (R) varies. When R = a cyano (CN) group, the cobamide is in its vitamin form; when R = 5'-deoxyadenosine, the cobamide is in its coenzymic form. The chemical nature of the lower (Co α) ligand base (B*) is diverse.⁵

subunits are evolutionarily related and share 37% and 57% amino acid identity and similarity, respectively. Furthermore, in addition to phenol and *p*-cresol, the enzyme converts DMB to α -DMB riboside monophosphate (α -ribazole-5'-phosphate or α -RP). The latter feature of ArsAB is noteworthy because, to date, none of the enzymes known to transfer DMB or any other nitrogenous base can utilize phenol or *p*-cresol.¹³ This feature of ArsAB is even more intriguing in light of the fact that both ArsA and ArsB proteins are homologues of the well-characterized nicotinate mononucleotide (NaMN):DMB phosphoribosyltransferase (CobT) enzyme of *Salmonella enterica* (*SeCobT*).¹² ArsA and ArsB share 37% and 36% amino acid sequence identity with *SeCobT*, but prior to this study it was unknown whether the phosphoribosyltransferase activity of ArsAB was provided by one or both subunits of the inferred heterodimer. The general scheme for the activation of the base is shown below in eq 1.



Crystallographic analyses of *SeCobT* (a homodimer) in complex with diverse substrates¹³ provided structural explanations for how the enzyme phosphoribosylates most of the nitrogenous bases found in cobamides, with the exception of phenol and *p*-cresol.

Here we report the three-dimensional crystal structure of *S. ovata* ArsAB in its substrate-free form (2.1 Å), and in complex with DMB (1.5 Å), *p*-cresol (2.1 Å), phloroglucinol (1.6 Å), and phenol (2.4 Å). Comparisons of the ArsAB complexes with the corresponding *SeCobT* complexes shed light onto the

subtle but profound evolutionary changes required for ArsAB to phosphoribosylate phenolic bases. Remarkably, only the active site in ArsA was occupied by substrate. Analysis of the ArsB active site identified an arginyl side chain that may block access to the site. The apparent inactivity of the ArsB subunit suggests a strictly structural role for ArsB in the phosphoribosyl transferase activity of this enzyme, though this does not preclude some other unidentified activity for that active site.

■ EXPERIMENTAL PROCEDURES

Construction of Plasmids Encoding ArsAB and Variants. The *arsA* and *arsB* coding sequences were amplified from plasmid pARSAB7¹² using primers listed in Table 1. The fragment was cut with *Sma*I and *Nhe*I enzymes and was ligated into the *Stu*I and *Nhe*I sites of plasmid pH6T, a pTEV5 derivative,¹⁴ yielding plasmid pARSAB22. Plasmid pARSAB22 directed the synthesis of H₆-ArsA and tag-less ArsB. Variants of ArsAB were constructed using the QuikChange method (Stratagene) using pARSAB22 as template. The plasmids constructed and primers used are listed in Table 1.

ArsAB Enzyme Isolation. ArsAB was overproduced using plasmid pARSAB22 in strain JE13607, a derivative of *E. coli* BL21(λ DE3) that lacks the *cobT* gene encoding the NaMN:5,6-dimethylbenzimidazole (DMB) phosphoribosyltransferase (CobT) enzyme of this bacterium. Strain JE13607 was used to ensure that native *E. coli* CobT protein did not contaminate the ArsAB heterodimer during subsequent kinetic analyses or interfere with protein folding.¹² Strain JE13607 harboring pARSAB22 was grown in six 2-L super broth (SB) medium cultures (tryptone 35 g, yeast extract 20 g, NaCl 5 g, NaOH 2N, 2.5 mL per liter of deionized H₂O). Expression of

Table 1. List of Plasmids and Primers Used in This Study

plasmid	genotype and description
pH6T	overexpression vector that fuses the N-terminus of the protein of interest to a H ₆ tag, which can be removed by rTEV protease, <i>bla</i> ⁺
pARSAB22	<i>So arsAB</i> ⁺ in pH6T, <i>bla</i> ⁺
pARSAB31	<i>So arsAB</i> ⁺ (ArsA M87Q) in pH6T, <i>bla</i> ⁺
pARSAB32	<i>So arsAB</i> ⁺ (ArsA I321S) in pH6T, <i>bla</i> ⁺
pARSAB33	<i>So arsAB</i> ⁺ (ArsA M87Q; I321S) in pH6T, <i>bla</i> ⁺
primer name	primer sequence
ArsA F	AGC TCG <u>CCC GGG</u> G ATG AGT TTA CTG CAA GCA ACA GTA GCG
ArsB R	GCA <u>GCT AGC</u> GCT TGC TAA TCT CTA ACA TCC TTG C
ArsA M87Q F	CCG ATA GAA ACA ACA ATT CAT CAG ACA GCT AAT TAT CTT ATC TC
ArsA M87Q R	GAG ATA AGA TAA TTA GCT GTC TGA TGA ATT GTT GTT TCT ATC GG
ArsA I321S F	CGG CTG GGA GAG GGT AGC GGG GCT TCT ATG GTT G
ArsA I321S R	CAA CCA TAG AAG CCC CGC TAC CCT CTC CCA GCC G

arsAB was induced by the addition of isopropyl- β -D-1-thiogalactopyranoside (IPTG, 0.5 mM) when cultures reached log-phase (~ 0.5 OD₆₀₀). After induction, cultures were shifted to 20 °C for 16 h. Cells were harvested by centrifugation (Beckman/Coulter Avanti J20-XPI refrigerated centrifuge, equipped with a JLA-8.1000 rotor; 15 min at 4 °C; 6000g), and frozen at -80 °C until used. Frozen pellets were resuspended in buffer A [50 mM 4-(2-hydroxyethyl)-1-piperazine-*N'*-(2-ethanesulfonic acid) (HEPES), pH 8], containing 300 mM NaCl, and 10 mM imidazole]; 1 mg/mL lysozyme and DNase were added to the cell suspension prior to disruption by sonication (60 s, 28% duty, 2 s pulses, setting 9) using a 500 Sonic Dismembrator (Fisher Scientific). Cell debris was removed by centrifugation (Beckman/Coulter Avanti J25-I refrigerated centrifuge, equipped with a JA-25.50 rotor; 45 min at 4 °C; 43000g). Clarified extract was applied onto an ÄKTA FPLC Purifier system (Amersham Biosciences) equipped with a 5-mL Ni-charged HisTrap fast flow (FF) column (GE Healthcare) equilibrated at a flow rate of 2 mL/min. After loading, the column was washed with 50 mL of buffer A before application of a 50-mL linear gradient of imidazole from 10 to 300 mM. Fractions containing ArsAB were pooled and His₇-tagged recombinant tobacco etch virus (His₇-rTEV) protease¹⁵ was added at 1:100 His₇-rTEV:ArsAB ratio to cleave the His₆ tag fused to ArsA.¹⁶ Tag-less ArsAB was reapplied onto the Ni-charged column to separate His₇-rTEV and other contaminants; tag-less ArsAB was found in the flow through. The ArsAB enzyme was dialyzed into 50 mM HEPES, pH 8.0, 100 mM NaCl, and 15% v/v glycerol then flash frozen in liquid nitrogen and stored at -80 °C until used.

Preparation of Variant Proteins. ArsAB variants encoded in pARSAB31, pARSAB32 and pARSAB33 were overexpressed in strain JE13607 in lysogenic broth (LB) as described above in 1-L scale. Clarified extracts in buffer A were applied onto a 1-mL bed volume of Ni-NTA Superflow resin (Qiagen) equilibrated with buffer A and washed with 10 column volumes of buffer A containing 20 mM imidazole. The variant enzymes were eluted with 10 column volumes of buffer A containing 300 mM imidazole. The His₆ tag fused to ArsA was cleaved as described above. Variant proteins were stored at -80 °C in the same buffer as wild type ArsAB until used.

Preparation of ArsAB Proteins for Crystallography.

For crystallographic studies, the concentration of NaCl and HEPES in ArsAB solutions was gradually reduced by dialysis (5 steps), from 50 mM HEPES pH 8.0 and 300 mM NaCl to 10 mM HEPES pH 7.5; the resulting solution was concentrated to 10 mg/mL before drop-freezing in liquid nitrogen. The concentration of ArsAB was determined using the combined calculated extinction coefficients of ArsA and ArsB at 280 nm (21150 cm⁻¹ M⁻¹) utilizing a NanoDrop 1000 spectrophotometer (Thermo).

Crystallization of ArsAB in the Substrate-Free State.

ArsAB heterodimers were screened for initial crystallization conditions by vapor diffusion at 25 and 4 °C with a 144-condition sparse matrix screen developed in the Rayment laboratory. Single, diffraction-quality crystals were grown by hanging drop vapor diffusion by mixing 2 μ L of 10 mg/mL ArsAB heterodimers in 10 mM HEPES pH 7.6 with 2 μ L of reservoir solution containing 100 mM 3-(*N*-morpholino)propanesulfonic acid (MOPS pH 7.1), 12.5% methyl ether polyethylene glycol 5000 (MEPEG5K), 20 mM NaCl, 12% ethylene glycol, and 10 mM phloroglucinol. Hanging droplets were immediately nucleated from an earlier spontaneous crystallization event with a cat's whisker. Crystals grew to approximate dimensions of 200 \times 200 \times 400 μ m within 7 days. Phloroglucinol was identified from an additive screen as a compound that dramatically improved the size, stability, and diffraction properties of the crystals. Subsequent structural studies showed that phloroglucinol binds in the active site of ArsA, which in hindsight is not surprising since it shares structural similarity to phenolic substrates. Additionally, phloroglucinol was found at low-occupancy in a different orientation in the corresponding ArsB site (Figure S1, Supporting Information). In order to prepare crystals of the substrate-free protein, the crystals were soaked in a solution containing 90 mM MOPS pH 7.1, 11.25% MEPEG5K, 25 mM NaCl, 12% ethylene glycol, and 25 mM imidazole for 1 week. The crystals of ArsAB were unstable in a synthetic mother liquor that lacked an aromatic base, however imidazole was not observed in the crystal lattice. The soaked crystals were transferred in two steps into a cryoprotectant solution which contained 100 mM MOPS pH 7.1, 12.5% MEPEG5K, 25 mM NaCl, 17% ethylene glycol, and 25 mM imidazole and rapidly plunged into liquid nitrogen. Substrate-free ArsAB crystallized in the space group $P2_12_12_1$ with unit cell dimensions of $a = 51.3$ Å, $b = 78.0$ Å, and $c = 151.8$ Å where there was a single ArsAB heterodimer in the asymmetric unit.

Crystallization of ArsAB Complexed With DMB.

Crystals were grown by mixing 2 μ L of ArsAB at 10 mg/mL containing 5 mM DMB, and 10 mM HEPES pH 7.6 with 2 μ L of reservoir solution containing 100 mM MOPS pH 7.1, 12.5% MEPEG5K, 20 mM NaCl, 12% ethylene glycol and 5 mM diethylenetriamine. Hanging droplets were nucleated immediately by streak-seeding where after the crystals grew to approximate dimensions of 200 \times 200 \times 400 μ m within 7 days. The crystals were transferred stepwise into a cryoprotecting solution containing 100 mM MOPS 7.1, 12.5% MEPEG5K, 20 mM NaCl, 15% ethylene glycol, and 5 mM diethylenetriamine and rapidly plunged into liquid nitrogen. ArsAB complexed with DMB crystallized in the space group $P2_1$ with unit cell dimensions of $a = 52.7$ Å, $b = 77.4$ Å, $c = 152.3$ Å, $\alpha = 90.0^\circ$, $\beta = 90.2^\circ$, and $\gamma = 90.0^\circ$ where there were two heterodimers of ArsAB in the asymmetric unit.

Table 2. X-ray Data Collection and Refinement Statistics

complex	phloroglucinol	phenol	<i>p</i> -cresol	substrate-free	DMB
pdb ID					
space group	$P2_12_12_1$	$P2_12_12_1$	$P2_12_12_1$	$P2_12_12_1$	$P2_1$
wavelength (Å)	0.979	1.54	0.979 Å	0.979 Å	0.979 Å
resolution range	50–0.150 (1.55–1.50) ^a	50–2.4 (2.45–2.4)	50–1.95 (1.98–1.95)	50–2.24 (2.28–2.24)	50–1.45 (1.48–1.45)
reflections: measured	1708377	223958	1052638	649606	1678842
reflections: unique	100980	24812	46511	30319	216492
redundancy	9.9 (3.4)	8.94 (5.7)	11.2 (5.7)	11.7 (5.4)	4.8 (3.3)
completeness (%)	99.7 (95.3)	99.5 (96.8)	99.4 (87.8)	99.4 (88.8)	97.6 (95.1)
average I/σ	47.0 (3.3)	26.8 (8.7)	49.8 (5.6)	47.0 (3.8)	36.9 (6.3)
R_{merge} (%) ^b	5.2 (40.0)	19.2 (52.8)	5.4 (38.2)	5.9 (54.8)	4.4 (22.9)
R_{work} ^c	18.9	20.5	19.4	20.5	18.6
R_{free} ^c	22.2	24.1	25.6	28.3	21.9
protein atoms	4839	9571	4794	4818	9892
ligand atoms	23	14	12	0	78
water molecules	546	204	186	105	1320
average B factors (Å ²)	23.373	22.343	42.122	57.298	23.151
Ramachandran (%)					
most favored	96.63	96.76	96.89	96.46	97.02
allowed	2.24	1.85	1.71	2.15	1.85
disallowed	1.12	1.39	1.40	1.38	1.13
rms deviations					
bond lengths (Å)	0.025	0.013	0.019	0.014	0.024
bond angles (deg)	2.538	1.808	2.042	1.718	2.45

^aValues in parentheses are for the highest-resolution shell. ^b $R_{\text{merge}} = (\sum |I_{\text{hkl}} - \bar{I}| \times 100.) / \sum I_{\text{hkl}}$ where the average intensity \bar{I} is taken over all symmetry equivalent measurements and I_{hkl} is the measured intensity for a given observation. ^c $R_{\text{factor}} = (\sum |F_{\text{obs}} - F_{\text{calc}}| \times 100.) / \sum |F_{\text{obs}}|$, where R_{work} refers to the R_{factor} for the data utilized in the refinement and R_{free} refers to the R_{factor} for 5% of the data that were excluded from the refinement.

Crystallization of ArsAB Complexed With *p*-Cresol.

Crystals of ArsAB in complex with *p*-cresol were prepared in a similar fashion to those required to obtain ArsAB in the substrate-free state with the exception that 20 mM *p*-cresol replaced the 25 mM imidazole in the soaking and cryoprotecting solutions. Crystals of ArsAB complexed with *p*-cresol belong to the space group $P2_12_12_1$ with unit cell dimensions of $a = 52.5$ Å, $b = 77.9$ Å, and $c = 152.2$ Å and contained a single ArsAB heterodimer in the asymmetric unit.

Crystallization of ArsAB Complexed With Phenol.

Crystals of ArsAB in complex with phenol were grown by combining 2 μL of 10 mg/mL ArsAB heterodimers in 10 mM HEPES pH 7.6 with 2 μL of reservoir solution containing 100 mM MOPS pH 7.1, 13.0% MEPEG5K, 20 mM NaCl, 12% ethylene glycol, and 25 mM phenol. Crystals were transferred stepwise into a cryoprotecting solution composed of 100 mM MOPS pH 7.1, 13.2% MEPEG5K, 17% ethylene glycol, and 25 mM phenol and frozen by rapidly plunging into liquid nitrogen. The crystals of ArsAB complexed with phenol belong to the space group $P2_12_12_1$ with unit cell dimensions of $a = 52.7$ Å, $b = 77.4$ Å, $c = 152.3$ Å, $\alpha = 90.0^\circ$, $\beta = 90.0^\circ$, and $\gamma = 90.0^\circ$ and two ArsAB heterodimers in the asymmetric unit.

Data Collection and Structure Determination for ArsAB Substrate-Free, DMB, *p*-cresol, and Phloroglucinol Complexes.

X-ray data for substrate-free ArsAB and ArsAB complexed with DMB, *p*-cresol, and phloroglucinol were collected at 100 K on the Structural Biology Center beamline 19BM at the Advanced Photon Source in Argonne, IL. Diffraction data were integrated and scaled with HKL3000.¹⁷ Data collection statistics are given in Table 2. The ArsAB heterodimer structure was determined using the structure of CobT from *Salmonella enterica* (PDB entry 1L4B) as a molecular replacement search model in the program Molrep.¹⁸

Final models were generated with alternate cycles of manual model building and least-squares refinement using the programs Coot¹⁹ and Refmac.²⁰ Refinement statistics are presented in Table 2.

Data Collection and Structure Determination for ArsAB Complexed with Phenol.

X-ray data for the ArsAB complexed with phenol were collected at 100 K with a Bruker AXS Platinum 135 CCD detector equipped with Montel optics and controlled by the Proteum software suite (Bruker AXS Inc.). All data sets were integrated with SAINT version 7.06A and internally scaled with SADABS version 2005/1. The structure was determined by molecular replacement using PHASER²¹ in which ArsAB from the DMB complex structure was used as a search model. Model refinement was performed by alternate cycles of manual building with Coot¹⁹ and restrained refinement with Refmac5.²² Refinement statistics are presented in Table 2.

ArsAB Kinetic Assays. Pseudo-first-order kinetics of the ArsAB-catalyzed reaction was performed using saturating concentrations of NaMN (5 mM), varying amounts of DMB or phenol (0.010–2 mM), and ArsAB protein at 0.25 μM. Stock solutions of DMB and phenol substrates were made in 30% (v/v) ethanol. All reaction mixtures contained 100 mM glycine pH 9 and 3% (v/v) ethanol at 37 °C. Triplicate assays were performed and analyzed as described elsewhere.¹²

ArsAB Activity Assays. Activities of ArsAB and variants on DMB and *p*-cresol were measured with 3 mM of substrates (DMB/*p*-cresol and NaMN) and 0.2 μg/μL enzyme in 100 mM glycine, pH 9.0. The amount of enzyme used in this assay was normalized to the least amount of variant protein needed to give detectable activity. Twenty-five microliters of each reaction was taken at 1, 6, and 13 min and boiled to stop the reaction. An equal volume of 20 mM ammonium acetate buffer

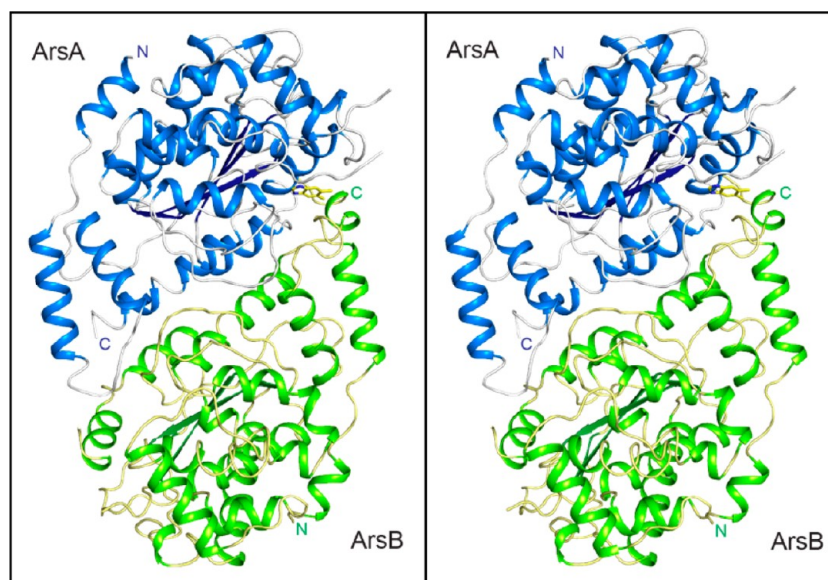


Figure 2. Stereo representation of ArsAB heterodimer. ArsA is colored in blue, ArsB is colored in green. DMB is shown in yellow.

pH 4.5 (buffer B) was added to each reaction, and the protein was filtered using a Spin-X column (Costar) before separation on the HPLC. The product of each reaction was separated on a Shimadzu Prominence UFLC equipped with a Kinetex 2.6 μm C18 100 \AA 100 \times 4.60 mm column (Phenomenex) at a flow rate of 0.8 mL/min. After injection, the column was developed for 0.6 min in 97% B and 3% acetonitrile (ACN) before a linear gradient to 60% B and 40% ACN over 6.4 min. Next, the column was developed for 3.2 min to 100% ACN and held at 100% ACN for 3.2 min. Retention times (minutes) were as follows: DMB, 9.7; *p*-cresol 11.2; α -DMB-riboside monophosphate, 7.4 and α -*p*-cresolyl-riboside monophosphate 7.6. Reactions were quantified against a standard curve derived from 0.1 - 30 nmol substrates.

RESULTS AND DISCUSSION

Identification of the Initiating Methionine of ArsA.

The initial characterization of the *S. ovata* *arsAB* genes identified two potential translational initiation sites in the *arsA*-coding region.¹² The difference between the two putative ArsA proteins was four amino acids (i.e., MEVI). In the previous report on ArsAB,¹² an overexpression vector (pARSAB7), was used to isolate an N-terminally tagged protein that included a hexahistidine (His_6) tag and a rTEV protease site followed by the MEVI residues mentioned above. The same vector also directed the synthesis of ArsB without a tag. After isolation of His_6 -ArsA, the His_6 -tag was removed with rTEV protease,¹⁵ leaving two additional glycines prior to the MEVI residues. ArsB copurified with ArsA, but the overproduction of ArsAB from pARSAB7 was poor under the conditions tested, and the enzyme could not be concentrated to more than 3 mg/mL (data not shown). This led to the question of whether the true start codon was the alternative methionine. Expression of *arsAB* from plasmid pARSAB22 eliminated the MEVI residues of ArsA but retained the His_6 affinity-tag and the rTEV enzyme recognition site. Protein expression driven by this construct yielded ArsAB enzyme that was readily purified under multiple conditions. Furthermore, the specific activity (nmol of product/min/mg of protein) of this material was 10-fold higher than that of the enzyme containing the additional

MEVI residues (274 vs 24, respectively). Finally, the resulting protein could be concentrated readily to more than 10 mg/mL.

Open reading frame (ORF) prediction software GeneMark.hmm also predicted the downstream translational start codon as the likely ORF for the gene.²³ The plasmid pARSAB22 was used to prepare ArsAB enzyme for all subsequent crystallographic and kinetic studies.

Structure of the Substrate-Free ArsAB Heterodimer.

Crystals of substrate-free ArsAB were obtained by soaking out the crystallization additive phloroglucinol, which bound in the ArsA active site. The final substrate-free-ArsAB model contains 334 of 348 expected amino acids for the ArsA subunit which extend from Ser2-Asn339. For the ArsB subunit the model contains 328 of 350 expected amino acid residues, which extend from Leu2-Ala333. The electron density is continuous for ArsA except for a break between Ser208 and Leu212 in ArsA. This disordered region consists of a loop that folds over the putative binding site for the substrate NaMN. In the ArsA subunit this loop is displaced by the N-terminus of a symmetry-related ArsB molecule in what is presumably a crystal packing interaction. The length of the break in this region varies among the substrate complexes determined. There is also one break in the electron density for ArsB between Ala70 and Met78. This break occurs in a surface loop that spans the active site cavity. The structure of substrate-free-ArsAB is shown in Figure 2.

Despite sharing only 37% sequence identity, ArsA and ArsB exhibit highly similar tertiary structures with a root-mean-square deviation (RMSD) of 1.3 \AA for 311 structurally equivalent α -carbon atoms. As expected, ArsA and ArsB have a very similar fold to that described for SeCobT²⁴ with an overall RMSD of 1.25 \AA with respect to either ArsA or ArsB relative to PDB coordinates 1D0S. The overall fold contains two domains where the large domain consists of a six-stranded parallel β -sheet surrounded by α -helices in the β_6 , β_5 , β_4 , β_1 , β_2 , β_3 arrangement characteristic of the classic Rossmann dinucleotide binding motif. The small domain is defined by a three-helix bundle, which is built from two N-terminal helices and a longer C-terminal helix that spans both domains.

The ArsAB heterodimer exhibits the same quaternary arrangement as the SeCobT homodimer, with numerous

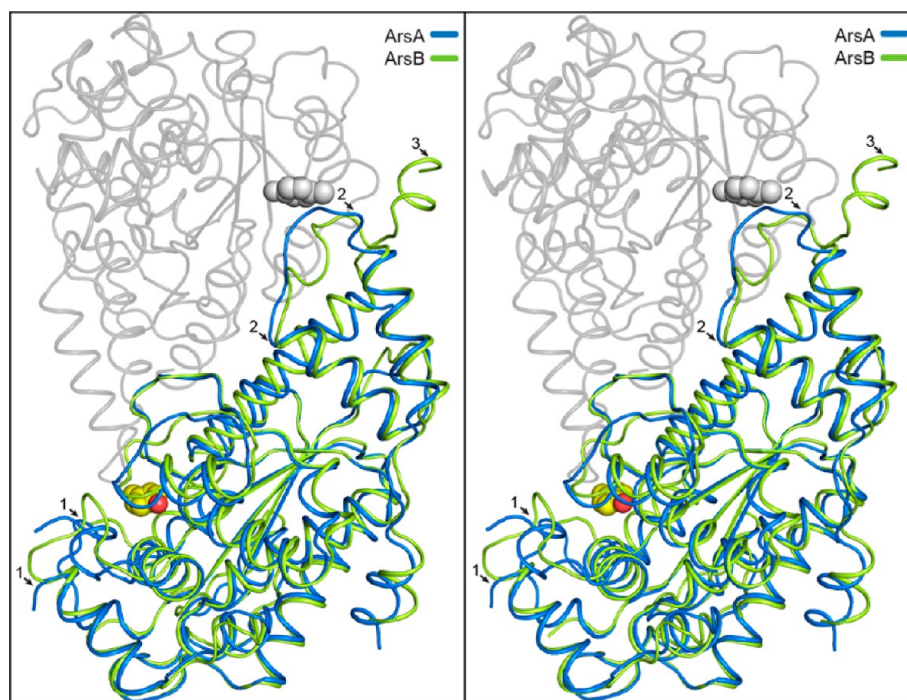


Figure 3. Structural alignment of ArsA with ArsB in stereo representation. ArsA (blue) with *p*-cresol bound (yellow) was superposed onto ArsB (green). The original positions of ArsA and *p*-cresol are depicted in light gray. Arrows indicate areas of greatest divergence: ¹ the loop that folds over the second substrate [ArsA: Gly206-Thr218, ArsB: Gly189-Gly197], ² the loop that projects into the active site on the adjacent subunit [ArsA: Val33-Gly41, ArsB: Leu27-His35], and ³ additional C-terminal helix in ArsB.

contacts along the dimer interface. The total buried surface area of the dimer is about 2300 Å²/subunit as computed with the program AREAIMOL in the ccp4 package.²⁵ In *SeCobT* and *ArsAB* the active site is located at the dimer interface and is built from both subunits of the dimer. The C-terminus of one subunit and a small N-terminal loop of the second subunit²⁴ form the site and result in two structurally equivalent active sites per dimer. Due to the heterodimeric nature of *ArsAB*, the two active sites in the dimer are structurally distinct.

There are notable structural differences in the surface loops that surround the active site cavities of *ArsA* and *ArsB*. The loop between helices 2 and 3 in *ArsB* (Leu27-Leu34) that forms part of the active site for *ArsA* curls away at Pro30 in *ArsB* in a fashion similar to that of *SeCobT* and provides sufficient room for substrate binding in the *ArsA* active site. Conversely, in *ArsB* the corresponding loop from *ArsA* penetrates further into the analogous site in *ArsB* (Figure 3). *ArsB* also contains an additional C-terminal helix spanning Phe327-Glu331 that projects from the three helix bundle of the small domain and is directed away from the *ArsA* active site. There is no observable electron density for the C-terminal 17 amino acids of *ArsB*. These differences, along with others discussed later, indicate that DMB phosphoribosyltransferase activity has been lost from the *ArsB* active site.

The observation that *ArsAB* heterodimers crystallized supports the earlier suggestion that neither *ArsA* nor *ArsB* can assemble independently to form an active enzyme.¹² *ArsAB* is likely the result of a gene duplication event onto which selective forces resulted in the coevolution of *ArsA* and *ArsB* into functional a heterodimer. Why functional homodimers were not favored remains unclear. At present, information available from genome databases shows that the tandem organization of *arsAB* is only found in some members of

Veillonellaceae family, suggesting that that the evolution of heterodimeric *SeCobT* homologues may be rooted in these bacteria.

Structure of *ArsAB* Heterodimer in Complex With DMB

The *ArsAB* heterodimer in complex with DMB crystallized in the space group *P2*₁ with two heterodimers in the asymmetric unit. No significant differences in tertiary structure were observed between the *ArsAB* heterodimer in either crystal system (RMSD: 0.45 Å), and inspection of the unit cell revealed no substantial change in crystal packing interactions. It is unclear whether the shift in space group was due to the presence of DMB, or by a change in crystallization conditions which included the crystallization additive diethylenetriamine.

There is unambiguous electron density for DMB in the *ArsA* active sites for both heterodimers in the asymmetric unit (Figure 4A). The overall RMSD between the two heterodimers in the asymmetric unit is 0.24 Å. Given the similarity between the two heterodimers, the discussion and figures are based on chains A and B in the asymmetric unit. The substrate binding site lies in a cavity at the interface of the *ArsA* and *ArsB* subunits, near the periphery of the dimer in a manner that is similar to that seen for *SeCobT*.²⁴ The cavity is defined by helices 5 and 6 and their connecting loop in *ArsA*, the loop leading into helix 16 in *ArsA*, and β4 and its adjoining loop in *ArsA*. Additionally, the loop between helices 2 and 3 of the *ArsB* subunit forms part of the cavity (Figure 4B). The cavity in which DMB binds is hydrophobic. DMB sits atop Met87 and Met177, Ile179, and Leu317 in *ArsA* and Pro30 in *ArsB*. An imidazole nitrogen on DMB forms a hydrogen bond with the proposed active site residue Glu319 (2.9 Å) (Glu317 in *SeCobT*).²⁶

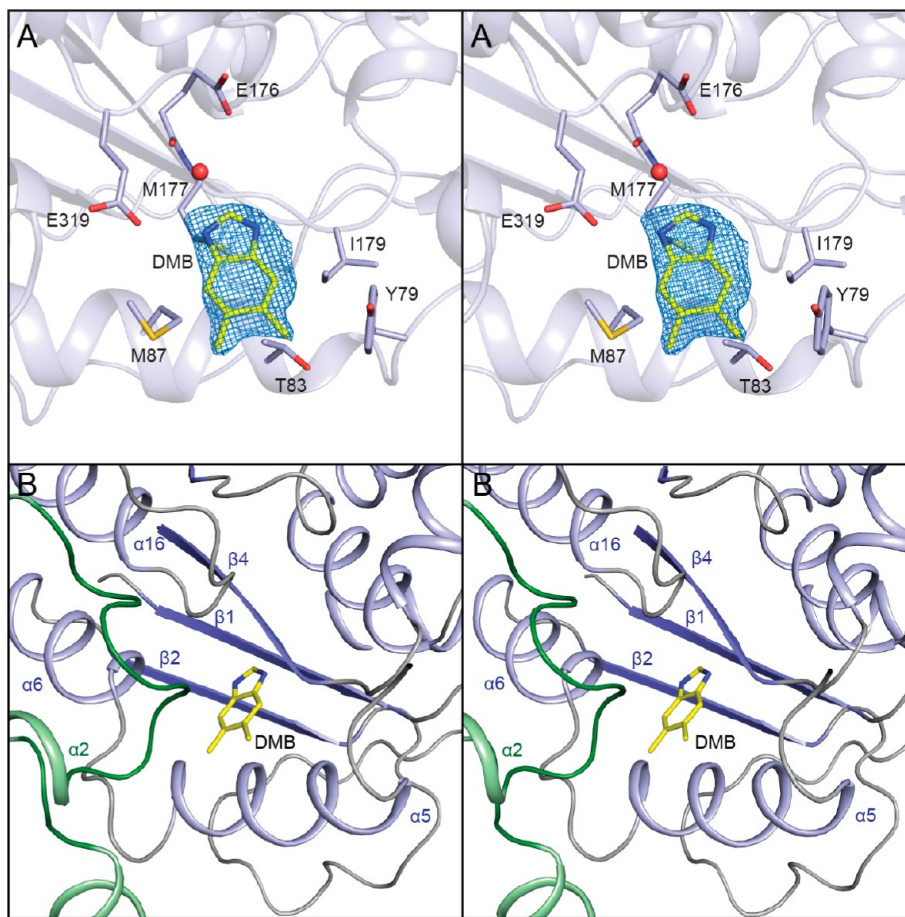


Figure 4. (A) Stereoview of the electron density for DMB in the ArsA active site. The electron density (3.5σ) was calculated from coefficients of the form $F_o - F_c$ where DMB was omitted from the phase calculation and refinement. ArsB has been omitted for clarity. (B) The DMB binding site is formed by contributions from both subunits: ArsA is shown in blue and ArsB is shown in green.

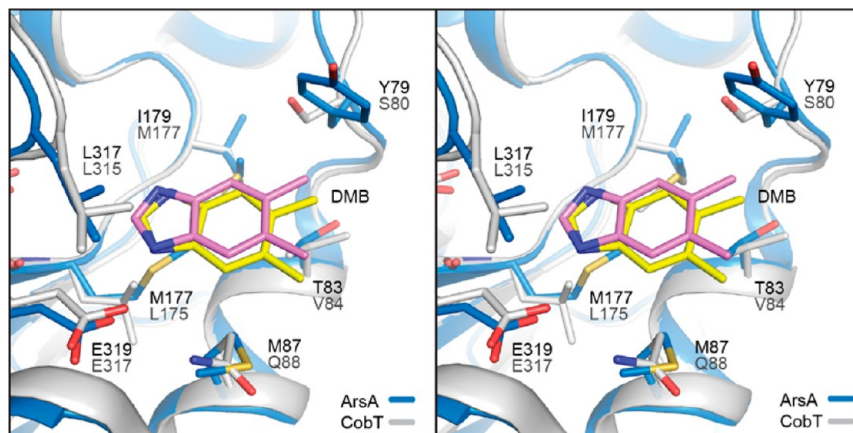


Figure 5. Alignment of SeCobT and ArsAB in complex with DMB. Coordinates for SeCobT·DMB were derived from PDB ID: 1D0S.²⁴ DMB from SeCobT is colored violet. DMB from ArsAB is colored yellow.

DMB Binding Is Conserved. Alignment of DMB-bound structures for ArsAB and SeCobT reveals that DMB binds in a nearly identical orientation in both enzymes (Figure 5). This is consistent with the sequence and structural conservation of the two enzymes. The character of most of the side chains in the DMB binding site are conserved between ArsA and SeCobT, many of which are hydrophobic. Notable exceptions are the substitution of both Gln88 and Leu175 in SeCobT to methionine in ArsA. These methionine residues form a large

part of the hydrophobic binding surface for DMB in ArsA. The most apparent difference in first shell interactions between SeCobT and ArsAB is the replacement of Ser80 in SeCobT with Tyr79 in ArsA. This substitution likely compensates for the absence of hydrophobic surface contributed by the C-terminus of SeCobT. There is no evidence that the largely disordered C-terminus of ArsB makes contacts with the active site of ArsA. Tyr79 of ArsA may play a role in the activation of phenolics as discussed later. A key conserved interaction in the active site of

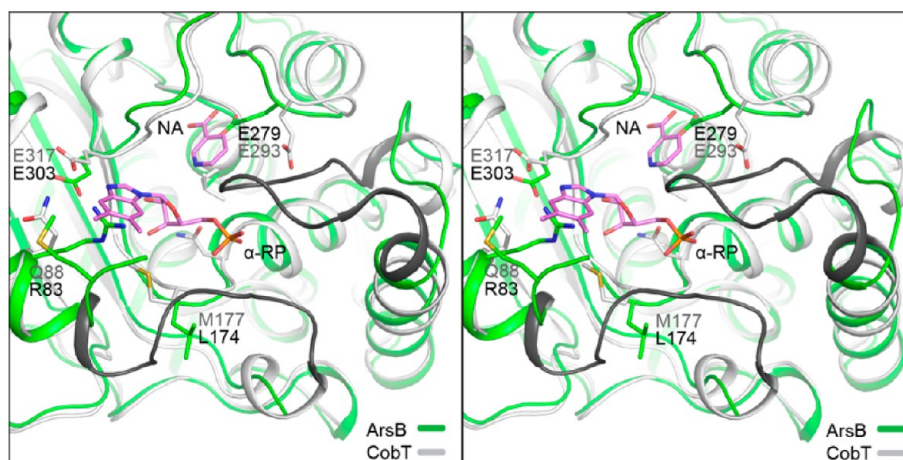


Figure 6. The active site of ArsB is inconsistent with NaMN:DMB phosphoribosyltransferase activity. This shows the alignment of SeCobT products complex with the ArsB active site. Coordinates for SeCobT in complex with its reaction products came from the PDB (accession number 1D0V).²⁴ α -Ribazole-5'-phosphate (α -RP) and nicotinate (NA) are colored violet. ArsB is colored green. SeCobT is colored gray. The loop that folds over the NaMN binding site in SeCobT is highlighted in dark gray. This loop is shortened by 11 residues in ArsB as can be seen in the far right of the image.

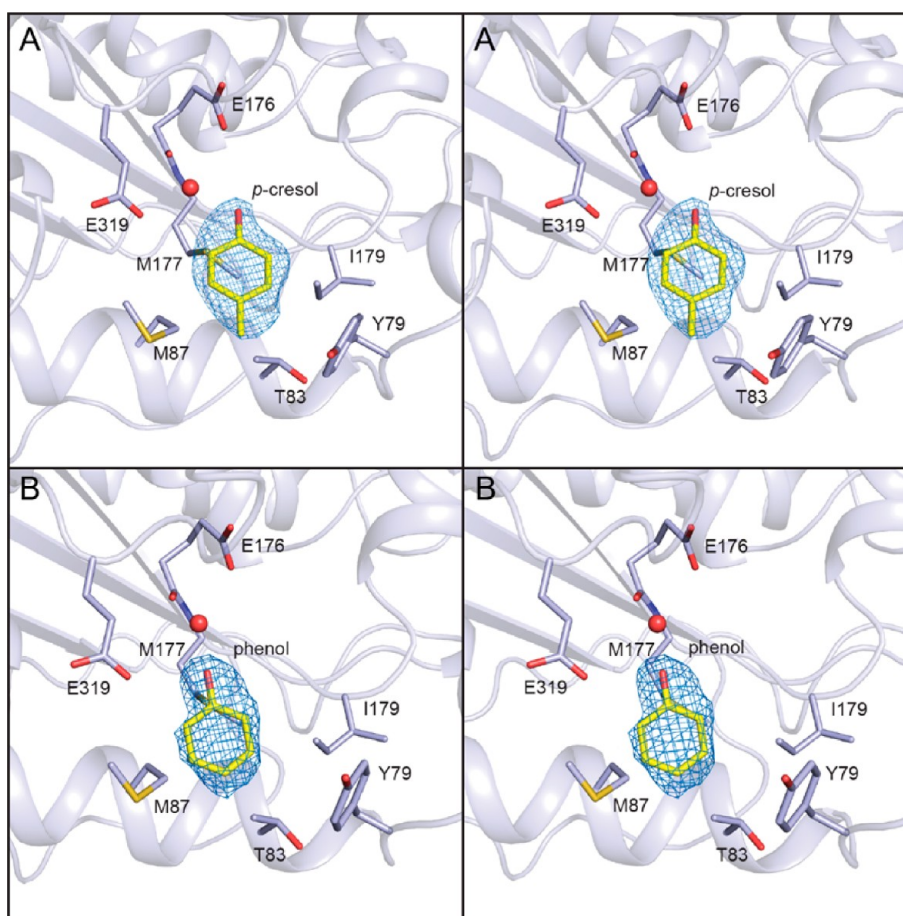


Figure 7. Stereoview for the electron density of (A) *p*-cresol and (B) phenol bound in the active site of ArsA. The electron density (3.0σ *p*-cresol, 2.0σ phenol) was calculated from coefficients of the form $F_o - F_c$ where *p*-cresol and phenol were omitted from the phase calculations and refinements. ArsB has been omitted for clarity.

ArsA is the hydrogen bond between Glu319 (Glu317 in SeCobT) and one of the imidazole nitrogen atoms of DMB. In addition to its role in coordinating and orienting the substrate, this residue has been proposed to act as an active site base²⁴ in SeCobT. This constellation of interactions is also observed in ArsAB providing strong evidence that ArsAB enzyme may

utilize the same catalytic mechanism as SeCobT to catalyze phosphoribosyl transfer.

The second substrate, NaMN, was not captured in complex with ArsAB. Indeed, the portion of the NaMN binding site in SeCobT that lies atop the phosphate moiety is disordered in the structurally equivalent region in ArsAB. This disordered loop

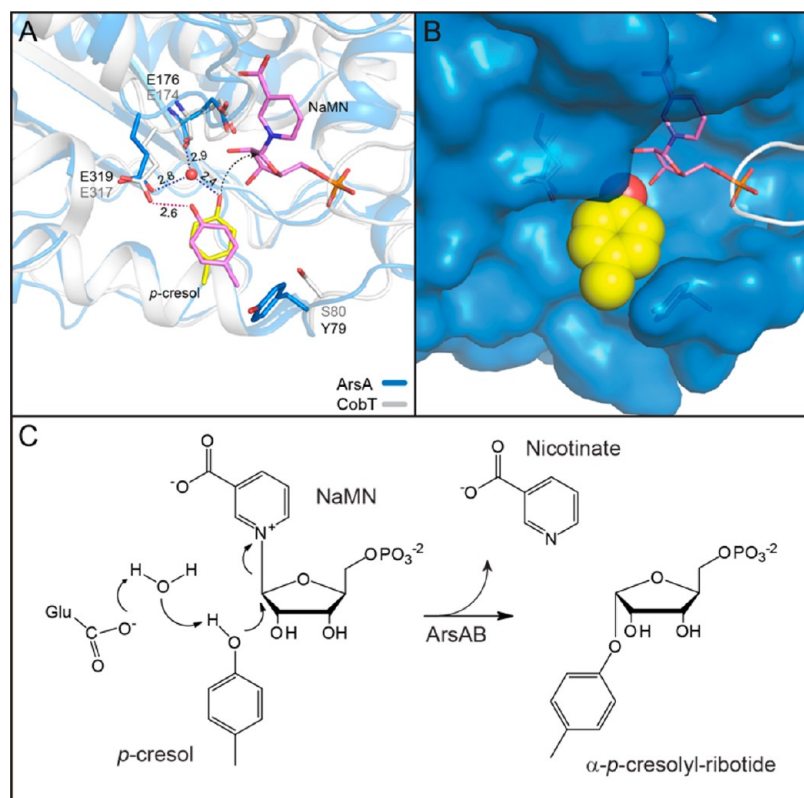


Figure 8. (A) Alignment of SeCobT and ArsAB in complex with *p*-cresol. Coordinates for SeCobT·*p*-cresol and for SeCobT·NaMN came from PDB accession numbers 1JHU and 1L4M respectively.¹³ *p*-Cresol is positioned by hydrogen bonds to an active site water molecule and the side chain of Tyr79. *p*-cresol (magenta) is bound to SeCobT, and *p*-cresol (yellow) is bound to ArsA. (B) A surface representation of ArsA and bound *p*-cresol shows that Tyr79 plays a role in positioning of the phenolic substrate. (C) Proposed mechanism for phenolic activation. ArsA is depicted in light blue whereas SeCobT is colored in white.

spans helices 9 and 10 in ArsA, and may undergo a disorder/order transition upon binding the second substrate. Alternatively, crystal-packing interactions may have displaced these residues as there are numerous contacts between the N-terminus of a symmetry related molecule of ArsB (Glu3 and Glu4) and the NaMN binding pocket in ArsA (Lys215). Despite the lack of structural information in this region, many key interactions, such as those between side chain of SeGlu174 and the amide nitrogen of SeGly176 with the ribose moiety are observed to be in structurally equivalent positions in ArsA (Glu179 and Gly 178). The cavity in which the nicotinate moiety binds is also maintained, however a slight rearrangement is observed around Ser293 in ArsA as compared to SeCobT, where SeSer291 interacts with an oxygen of the carboxylate group of nicotinate. In ArsA, the peptide backbone of the Ser293 has rotated nearly 180° leaving the side chain directed toward the solvent rather than the nicotinate binding cavity.

DMB Phosphoribosyl Transferase Activity Is not Maintained in ArsB. While there is a strong conservation of active site architecture and substrate binding between SeCobT and ArsA, the equivalent site in ArsB shows considerable divergence (Figure 6). The most striking difference is the position of the side chain of Arg83, which lies directly within the DMB binding site. Additionally, the hydrophobic loop that is contributed by the adjacent ArsA subunit lies much deeper in the cavity and is not curled away from the site by Pro30 (ArsB) as is observed in the ArsA DMB binding site. Considered together, these structural features of ArsAB likely preclude the

binding of DMB in a conformation that is catalytically competent. Interestingly, the proposed catalytic residue Glu303 is maintained in a structurally equivalent position in ArsB. The NaMN-binding site has also undergone several structural rearrangements as depicted in Figure 6. The loop that folds over the phosphate moiety in NaMN in SeCobT is shortened in ArsB and tracks along the outer surface of the cavity rather than toward the interior. A sequence alignment of SeCobT and ArsB shows an 11 residue gap in this region in ArsB. Lastly, the loop that includes Tyr79 in ArsA and spans β 1 and helix 4 is disordered in ArsB but is directed inward toward the active site cavity before becoming disordered. The structural divergence of the active site in ArsB could be the result of selective pressures leading to heterodimer formation, or to the ability of ArsA to transfer phenolic bases. At this point, it is unknown whether the ArsB site has any catalytic activity whatsoever. It is conceivable that the ArsB active site has evolved to perform another function. In this respect, although the ArsB active site does not have base:phosphorylribosyl transferase activity, the presence of phloroglucinol (Figure S1, Supporting Information) in the ArsB active site suggests that the capacity to bind phenolic bases has been maintained.

Structure of ArsAB Heterodimer in Complex with Phenol and *p*-Cresol. To gain insight into the mechanism by which ArsAB generates phenolic α -riboside monophosphates, crystal structures were determined for ArsAB in complex with both *p*-cresol and phenol. There is clear electron density in the ArsA active site for both substrates (Figure 7). The phenolic substrates bind in the same location in the active site cavity at

the interface between the ArsA and ArsB subunits. The constellation of side chains surrounding the bound substrate remains unchanged relative to the complex with DMB with the notable exception of the hydrogen bonding pattern about Glu319 and the loop between helices 4 and 5, most notably at Tyr79. While Glu319 participates in a direct hydrogen bond with the imidazole nitrogen in complex DMB (2.9 Å), it has been replaced with a well-ordered water molecule with phenolic substrates bound. In the case of *p*-cresol, this water molecule (W1) is 2.8 Å from O ϵ 2 of Glu319 and 2.4 Å from the hydroxyl moiety on *p*-cresol (Figure 8). The presence of W1 results in a rotation of the planar substrate away from Glu319 and toward the NaMN binding site. This position is additionally maintained by the rotation of Tyr79 3.6 Å inward from that of the DMB complex, resulting in a close interaction with *p*-cresol (Figure 8). Taken together, these interactions likely explain how *p*-cresol is positioned for a nucleophilic attack at the C1 carbon of ribose following deprotonation, which is facilitated by the close hydrogen bond with W1, as it is ideally positioned to transfer a proton to Glu319.

Comparison of SeCobT with ArsAB Bound to Phenolic Substrates. SeCobT is unable to catalyze phosphoribosyl transfer to phenolic substrates, whereas this is readily accomplished by ArsAB. The presence of a water molecule in the active site of the ArsAB:phenolic complexes compared to the absence of a water molecule in the phenolic complexes with SeCobT suggests that a water molecule plays a key role in the positioning and deprotonation of *p*-cresol for attack at the C1 carbon of ribose. In SeCobT, *p*-cresol hydrogen bonds directly (2.6 Å) with O ϵ 2 of Glu317. This close hydrogen bond between *p*-cresol and Glu317, places the phenolic hydroxyl group in a position that is most likely too far from the C1 carbon of ribose (>4.0 Å) for the reaction to occur. The reason that SeCobT does not allow inclusion of a water molecule in the equivalent position of W1 in ArsAB is not immediately obvious, but careful examination of the comparison of the active sites in ArsAB and SeCobT suggests several possibilities.

Superposition of the active sites (Figure 9) shows that in order for ArsA to accommodate a water molecule the catalytic glutamate Glu319 (Glu317 in SeCobT) must move away from its position in SeCobT. This would appear to be facilitated by the replacement of Gln88 in SeCobT by Met87 in ArsA. This change removes a hydrogen bonding interaction which is predicted to stabilize the position of the catalytic glutamate in the active site. There is also a difference in the position and conformation of the backbone atoms for the polypeptide chain that surrounds the catalytic base. This change appears to be coupled to a number of changes in this region. In particular, replacement of Ser319 in SeCobT by Ile321 in ArsA requires a rearrangement in the backbone to accommodate the loss of a hydrogen bond.

The hypothesis that Met87 and Ile321 play a role in enabling ArsAB to catalyze phosphoribosyl transfer to phenolic substrates was tested by preparing the reverse mutations M87Q and I321S (Table 3). The effect of the M87Q mutation is most pronounced with respect to phenolic specificity, as the specific activity with *p*-cresol drops by 2.6 fold while a slight increase (1.2 fold) in activity with DMB was observed. Introduction of serine at Ile321 was deleterious to both phenolic and DMB activation, suggesting that the role of this amino acid residue in ArsA is not well understood. From these experiments it is clear that specificity for phenolic substrates is influenced by more

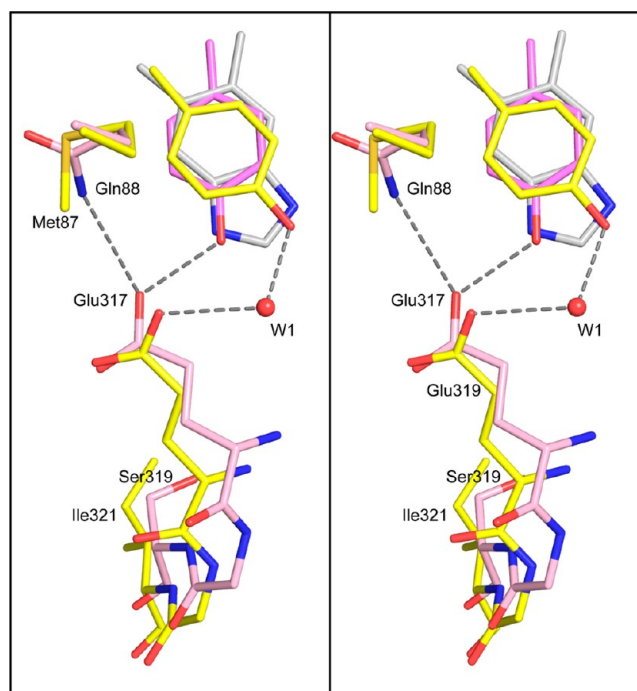


Figure 9. Inclusion of a water molecule in the active site of ArsA. Structural overlay of ArsAB and SeCobT complexed with *p*-cresol shows that subtle changes in the position of the catalytic glutamate allow the incorporation of a water molecule into the active site of ArsA. It is hypothesized that these differences are facilitated by removal of a hydrogen bond in the active site (replacement of a glutamine by a methionine) and conformational changes in the backbone associated with Ile321. The coordinates of SeCobT complexed with *p*-cresol were taken from PDB accession number 1JHU.¹³

than one residue of the base-binding pocket. A full understanding of the structural basis for the utilization of phenolic substrates by ArsAB must await further structural and kinetic studies of variants.

Efficiency of the ArsAB Enzyme as a Function of its Base Substrate. Earlier work by Stupperich et al. showed that *p*-cresolyl-Cba and phenolyl-Cba comprised >90% of the cobamides synthesized by *S. ovata*,^{8,9} yet data shown in Table 4 indicate that the ArsAB enzyme efficiently uses DMB as its base substrate. However, the K_M of ArsAB for DMB reported herein (415 μ M) is much higher than other CobT homologues, namely *S. enterica* ($K_M < 10 \mu$ M) and *Pseudomonas denitrificans* (16 nM).^{27,28} The dramatic increase in K_M for DMB in ArsAB may be a consequence of the evolutionary changes required for this enzyme to phosphoribosylate phenolic bases. From this perspective the higher K_M for DMB observed with ArsAB suggests that increased flexibility needed to accommodate a water molecule might be a compromise to maintain both activities. The crystallographic snapshots of ArsAB and SeCobT show DMB bound in the same position and orientation in both enzyme active sites so there is no easy structural explanation for the observed difference in K_M between ArsAB and SeCobT. Interestingly, the interaction between the C-terminal residues contributed by the neighboring subunit in SeCobT and DMB are apparently lacking in ArsAB. This could affect on-rates and off-rates of substrate and thereby K_M .

The catalytic efficiency of the activation of DMB and phenol for ArsAB differ only by a factor of 2 (Table 4), suggesting that,

Table 3. Specific Activities for Variants of ArsA towards DMB and *p*-Cresol^a

substrate	wild type	M87Q	I321S	M87Q/I321S
<i>p</i> -cresol	37.6 ± 0.8	14.2 ± 1.6	8.3 ± 1.7	0.7 ± 0.1
5,6-dimethylbenzimidazole	160.7 ± 7.9	192.6 ± 12.2	16.7 ± 1.9	2.4 ± 1.0

^aSpecific activities are represented in nmol product formed/min/mg enzyme, from 1 to 13 min, three time points taken to ensure linearity, averages and standard deviations taken from three replicate reactions.

Table 4. Kinetic Parameters of the ArsAB-Catalyzed Reaction^a

substrate	K_M (μ M)	k_{cat} (s^{-1})	k_{cat}/K_M ($s^{-1} M^{-1}$)
5,6-dimethylbenzimidazole	415 ± 56	1.6 ± 0.08	3.9×10^3
phenol	50 ± 11	0.4 ± 0.05	8×10^3

^aReaction mixtures contained either 1.9 mM phenol + [¹⁴C-U]-phenol (0.1 mM, 60 mCi mmol⁻¹), or 1.98 mM 5,6-dimethylbenzimidazole (DMB) + [¹⁴C-2]-DMB (0.02 mM, 43 mCi mmol⁻¹). Other components present in the reaction mixture and the protocol for the assessment of product formation are described under Experimental Procedures.

under some conditions, this bacterium may synthesize cobalamin (Co β -5,6-dimethylbenzimidazolyl-Cba) or other cobamides containing purines or purine analogues.^{5,12} Notably, while the apparent K_M for phenol was 8-fold lower than the apparent K_M for DMB, the turnover number when phenol was the substrate was 4-fold slower than the one calculated for the reaction when DMB was the substrate (Table 4). It is noteworthy that phenolyl-Cba comprises only 20% of the pool of phenolic-Cbas synthesized by *S. ovata* so that the kinetic parameters for phenol could differ from those for *p*-cresol. The kinetic parameters for *p*-cresol were not measured because ¹⁴C-*p*-cresol necessary for the kinetic assay developed and used in this study is not commercially available.

CONCLUSIONS

The structural studies described here confirm that the ArsAB heterodimer from *Sporomusa ovata* contains one functional active site for nicotinate mononucleotide:phenol/*p*-cresol phosphoribosyltransferase, which is formed mostly by amino acid residues from the ArsA subunit. The role of the ArsB subunit is unclear; though it does retain the ability to weakly bind phenolic bases, which allows the possibility that this component of the protein has evolved a new but unknown function. The complexes of ArsAB with phenol and *p*-cresol suggest that ArsAB has evolved to accommodate phosphoribosyl transfer to phenolic substrates by allowing a water molecule to enter into the active site. This water molecule serves to reposition phenolic substrates such that the hydroxyl moiety is closer to the putative location of the C1 carbon on ribose which is predicted to facilitate nucleophilic attack. Comparison of the structure of ArsAB with the NaMN:DMB phosphoribosyltransferase (CobT) enzyme of *Salmonella enterica* suggests that comparatively few changes are required to facilitate phosphoribosyl transfer to phenolic substrates.

ASSOCIATED CONTENT

Supporting Information

A stereoview of the electron density for phloroglucinol (pho) bound to ArsB in the complex of ArsAB with phloroglucinol. This material is available free of charge via the Internet at <http://pubs.acs.org>.

Accession Codes

X-ray coordinates for the substrate-free form and in complex with DMB, *p*-cresol, phloroglucinol, and phenol have been deposited in the Research Collaboratory for Structural Bioinformatics, Rutgers University, New Brunswick, N. J. (Protein Data Bank entries 4HDN, 4HDR, 4HDM, 4HDK, and 4HDS respectively)

AUTHOR INFORMATION

Corresponding Author

* (I.R.) Department of Biochemistry, University of Wisconsin, 433 Babcock Dr., Madison, WI 53706; phone, (608) 262-0437; fax, (608) 262-1319; e-mail, ivan_rayment@biochem.wisc.edu. (J.C.E.-S.) Department of Microbiology, University of Georgia, 527 Biological Sciences Building, 120 Cedar Street, Athens, GA 30602, phone, (706) 542 2651; fax, 706 542 2815; e-mail jcescala@uga.edu.

Author Contributions

[§]These authors contributed equally to this work.

Funding

This work was supported in part by NIH Grants GM083987 and GM086351 to I.R. and R37 GM40313 to J.C.E.-S. Use of the SBC 19 μ B beamline at the Argonne National Laboratory Advanced Photon Source was supported by the U.S. Department of Energy, Office of Energy Research, under Contract No. W-31-109-ENG-38.

Notes

The authors declare no competing financial interest.

ABBREVIATIONS USED

Ado, adenosyl; cobamide, Cba; 5,6-dimethylbenzimidazole, DMB; nicotinate mononucleotide, NaMN; 4-(2-hydroxyethyl)-1-piperazine-*N'*-(2-ethanesulfonic acid, HEPES; methyl ether polyethylene glycol 5000, MEPEG5K; NaMN, DMB phosphoribosyltransferase (CobT) enzyme of *Salmonella enterica*, (SeCobT); 3-(*N*-morpholino)propanesulfonic acid, MOPS; root-mean-square deviation, RMSD

REFERENCES

- (1) Battersby, A. R. (2000) Tetrapyrroles: the pigments of life. *Nat. Prod. Rep.* 17, 507–526.
- (2) Banerjee, R. (2003) Radical carbon skeleton rearrangements: catalysis by coenzyme B12-dependent mutases. *Chem. Rev.* 103, 2083–2094.
- (3) Yamanishi, M., Yunoki, M., Tobimatsu, T., Sato, H., Matsui, J., Dokiya, A., Iuchi, Y., Oe, K., Suto, K., Shibata, N., Morimoto, Y., Yasuoka, N., and Toraya, T. (2002) The crystal structure of coenzyme B12-dependent glycerol dehydratase in complex with cobalamin and propane-1,2-diol. *Eur. J. Biochem.* 269, 4484–4494.
- (4) Matthews, R. G., Koutmos, M., and Datta, S. (2008) Cobalamin-dependent and cobamide-dependent methyltransferases. *Curr. Opin. Struct. Biol.* 18, 658–666.
- (5) Renz, P. (1999) Biosynthesis of the 5,6-dimethylbenzimidazole moiety of cobalamin and of other bases found in natural corrinoids, in *Chemistry and Biochemistry of B12* (Banerjee, R., Ed.) pp 557–575, John Wiley & Sons, Inc., New York.

- (6) Yi, S., Seth, E. C., Men, Y. J., Stabler, S. P., Allen, R. H., Alvarez-Cohen, L., and Taga, M. E. (2012) Versatility in Corrinoid Salvaging and Remodeling Pathways Supports the Corrinoid-Dependent Metabolism of *Dehalococcoides mccartyi*. *Appl. Environ. Microbiol.* 78, 7745–7752.
- (7) Escalante-Semerena, J. C., Warren, M. J. (2008) Biosynthesis and Use of Cobalamin (B₁₂), in *EcoSal - Escherichia coli and Salmonella: Cellular and Molecular Biology* (Böck, A., Curtiss III, R., Kaper, J. B., Karp, P. D., Neidhardt, F. C., Nyström, T., Slauch, J. M., Squires, C. L., Eds.) ASM Press, Washington, D. C.
- (8) Stupperich, E., Eisinger, H. J., and Kräutler, B. (1989) Identification of phenolyl cobamide from the homoacetogenic bacterium *Sporomusa ovata*. *Eur. J. Biochem.* 186, 657–661.
- (9) Stupperich, E., Eisinger, H. J., and Kräutler, B. (1988) Diversity of corrinoids in acetogenic bacteria. *p*-Cresolylcobamide from *Sporomusa ovata*, 5-methoxy-6-methylbenzimidazolylcobamide from *Clostridium formicoaceticum* and vitamin B₁₂ from *Acetobacterium woodii*. *Eur. J. Biochem.* 172, 459–464.
- (10) Abend, A., Bandarian, V., Nitsche, R., Stupperich, E., Reteý, J., and Reed, G. H. (1999) Ethanolamine ammonia-lyase has a “base-on” binding mode for coenzyme B₁₂. *Arch. Biochem. Biophys.* 370, 138–141.
- (11) Poppe, L., Stupperich, E., Hull, W. E., Buckel, T., and Réteý, J. (1997) A base-off analogue of coenzyme-B₁₂ with a modified nucleotide loop—1H-NMR structure analysis and kinetic studies with (R)-methylmalonyl-CoA mutase, glycerol dehydratase, and diol dehydratase. *Eur. J. Biochem.* 250, 303–307.
- (12) Chan, C. H., and Escalante-Semerena, J. C. (2011) ArsAB, a novel enzyme from *Sporomusa ovata* activates phenolic bases for adenosylcobamide biosynthesis. *Mol. Microbiol.* 81, 952–967.
- (13) Cheong, C. G., Escalante-Semerena, J. C., and Rayment, I. (2001) Structural investigation of the biosynthesis of alternative lower ligands for cobamides by nicotinate mononucleotide: 5,6-dimethylbenzimidazole phosphoribosyltransferase from *Salmonella enterica*. *J. Biol. Chem.* 276, 37612–37620.
- (14) Rocco, C. J., Dennison, K. L., Klenchin, V. A., Rayment, I., and Escalante-Semerena, J. C. (2008) Construction and use of new cloning vectors for the rapid isolation of recombinant proteins from *Escherichia coli*. *Plasmid* 59, 231–237.
- (15) Blommel, P. G., and Fox, B. G. (2007) A combined approach to improving large-scale production of tobacco etch virus protease. *Protein Expr. Purif.* 55, 53–68.
- (16) Blommel, P. G., Becker, K. J., Duvnjak, P., and Fox, B. G. (2007) Enhanced bacterial protein expression during auto-induction obtained by alteration of *lac* repressor dosage and medium composition. *Biotechnol. Prog.* 23, 585–598.
- (17) Otwinowski, Z., and Minor, W. (1997) Processing of X-ray diffraction data collected in oscillation mode. *Methods Enzymol.* 276, 307–326.
- (18) Vagin, A., and Teplyakov, A. (2000) An approach to multi-copy search in molecular replacement. *Acta Crystallogr. D Biol. Crystallogr.* 56, 1622–1624.
- (19) Emsley, P., and Cowtan, K. (2004) Coot: model-building tools for molecular graphics. *Acta Crystallogr. D Biol. Crystallogr.* 60, 2126–2132.
- (20) Murshudov, G. N., Vagin, A. A., and Dodson, E. J. (1997) Refinement of macromolecular structures by the Maximum-Likelihood Method. *Acta Crystallogr. D Biol. Crystallogr.* 53, 240–255.
- (21) McCoy, A. J., Grosse-Kunstleve, R. W., Adams, P. D., Winn, M. D., Storoni, L. C., and Read, R. J. (2007) Phaser crystallographic software. *J. Appl. Crystallogr.* 40, 658–674.
- (22) Murshudov, G. N., Skubak, P., Lebedev, A. A., Pannu, N. S., Steiner, R. A., Nicholls, R. A., Winn, M. D., Long, F., and Vagin, A. A. (2011) REFMAC5 for the refinement of macromolecular crystal structures. *Acta Crystallogr. D Biol. Crystallogr.* 67, 3553–3567.
- (23) Lukashin, A. V., and Borodovsky, M. (1998) GeneMark.hmm: new solutions for gene finding. *Nucleic Acids Res.* 26, 1107–1115.
- (24) Cheong, C. G., Escalante-Semerena, J. C., and Rayment, I. (1999) The three-dimensional structures of nicotinate mononucleotide:5,6-dimethylbenzimidazole phosphoribosyltransferase (CobT) from *Salmonella typhimurium* complexed with 5,6-dimethylbenzimidazole and its reaction products determined to 1.9 Å resolution. *Biochemistry* 38, 16125–16135.
- (25) Winn, M. D., Ballard, C. C., Cowtan, K. D., Dodson, E. J., Emsley, P., Evans, P. R., Keegan, R. M., Krissinel, E. B., Leslie, A. G., McCoy, A., McNicholas, S. J., Murshudov, G. N., Pannu, N. S., Potterton, E. A., Powell, H. R., Read, R. J., Vagin, A., and Wilson, K. S. (2011) Overview of the CCP4 suite and current developments. *Acta Crystallogr., Sect. D* 67, 235–242.
- (26) Cheong, C. G., Escalante-Semerena, J. C., and Rayment, I. (2002) Capture of a labile substrate by expulsion of water molecules from the active site of nicotinate mononucleotide:5,6-dimethylbenzimidazole phosphoribosyltransferase (CobT) from *Salmonella enterica*. *J. Biol. Chem.* 277, 41120–41127.
- (27) Trzebiatowski, J. R., and Escalante-Semerena, J. C. (1997) Purification and characterization of CobT, the nicotinate-monomonucleotide:5,6-dimethylbenzimidazole phosphoribosyltransferase enzyme from *Salmonella typhimurium* LT2. *J. Biol. Chem.* 272, 17662–17667.
- (28) Cameron, B., Blanche, F., Rouyez, M. C., Bisch, D., Famechon, A., Couder, M., Cauchois, L., Thibaut, D., Debussche, L., and Crouzet, J. (1991) Genetic analysis, nucleotide sequence, and products of two *Pseudomonas denitrificans* *cob* genes encoding nicotinate-nucleotide: dimethylbenzimidazole phosphoribosyltransferase and cobalamin (5'-phosphate) synthase. *J. Bacteriol.* 173, 6066–6073.